



1-Aminoanthraquinone as an electro-polymerizable additive to improve the cycling performance of a $\text{Na}_3\text{V}_2(\text{PO}_4)_2\text{F}_3$ cathode

Myung-Soo Park¹, Jin-Yi Choi¹, Ganesh Kumar Veerasubramani, Dong-Won Kim*

Department of Chemical Engineering, Hanyang University, Seongdong-Gu, Seoul 04763, Republic of Korea

ARTICLE INFO

Keywords:

Electrolyte additive
Conductive polymer
Electro-oxidative polymerization
Sodium-ion battery
Poly(1-aminoanthraquinone)

ABSTRACT

A small amount of 1-aminoanthraquinone (AAQ) was used as an electro-polymerizable additive in a liquid electrolyte. AAQ was electrochemically oxidized to form a thin conductive poly(1-aminoanthraquinone) (PAAQ) layer on a sodium-ion cathode material, $\text{Na}_3\text{V}_2(\text{PO}_4)_2\text{F}_3$ (NVPF), at approximately 4.0 V during the initial charging processes. The resulting PAAQ layer provided an effective conduction pathway in the NVPF electrode, and thus enhanced the cycling performance in terms of the discharge capacity, cycling stability and rate capability. Our study demonstrates a simple and efficient approach to boost the electrochemical performance of a NVPF cathode for sodium-ion batteries.

1. Introduction

Considering the natural abundance and low cost of sodium resources in the world, sodium-ion batteries (SIBs) are a promising alternative to lithium-ion batteries (LIBs) in the application of large-scale energy storage systems [1–4]. However, SIBs have lower energy density than LIBs because of the larger atomic mass of sodium and higher redox potential of Na/Na^+ (-2.71 V vs. SHE) compared with Li counterparts [4]. To overcome this drawback, many cathode materials with high redox potential and high specific capacity, including $\text{P2-Na}_{0.55}[\text{Ni}_{0.1}\text{Fe}_{0.1}\text{Mn}_{0.8}]\text{O}_2$, $\text{P2-Na}_{2/3}[\text{Mg}_{0.28}\text{Mn}_{0.72}]\text{O}_2$, $\text{Na}_3\text{V}_2\text{O}_{2x}(\text{PO}_4)_2\text{F}_{3-2x}$, $\text{Na}_3\text{V}_2(\text{PO}_4)_2\text{F}_3$ (NVPF) and $\text{Na}_4\text{Co}_3(\text{PO}_4)_2\text{P}_2\text{O}_7$, have been investigated for use in SIBs [5–10]. Among them, NVPF with a NASICON structure (Na superionic conductor) that enables fast Na^+ diffusion has been recognized as a potential cathode material because of its high theoretical capacity (128 mAh g^{-1}), structural stability and high operating voltage [11,12]. However, its electronic conductivity is quite low ($\sim 10^{-12} \text{ S cm}^{-1}$); therefore, improving the rate performance of the NVPF material is a challenge for its practical application in SIBs. To date, various studies on the synthesis of NVPF-carbon composites with high electronic conductivity have reported to improve charge transfer reaction kinetics and cycling performance [11–18]. Though these approaches could enhance the electrochemical performance of NVPF, they require additional carbon sources and time-consuming steps.

In this study, we report the electrochemical oxidation of 1-aminoanthraquinone (AAQ) to form the electron-conductive poly(1-

aminoanthraquinone) (PAAQ) on the surface of NVPF to enhance its electrochemical performance. AAQ was chosen as an electro-polymerizable additive, because it can be electrochemically oxidized in the working potential range of the NVPF [19]. The thin PAAQ layer formed on NVPF could provide an electron conduction pathway and facilitate electron transfer in the cathode. As a result, the NVPF electrode employing an optimum amount of AAQ exhibited lower interfacial resistance and enhanced high rate performance. To the best of our knowledge, this is the first report on the *in-situ* formation of an electronically-conductive polymer on NVPF material for SIBs.

2. Experimental

2.1. Electrolyte

NaClO_4 (anhydrous, 99.5%, Alfa Aesar) was used after vacuum drying at 120°C for 24 h. Ethylene carbonate (EC, anhydrous, 99.0%, Sigma-Aldrich) and propylene carbonate (PC, anhydrous, 99.7%, Sigma-Aldrich) were used as electrolyte solvents. Fluoroethylene carbonate (FEC, battery grade, Enchem) was used as a solid electrolyte interphase (SEI)-forming additive in the electrolyte. AAQ (> 98.0%, TCI) was used after vacuum drying at 80°C for 24 h. The electrolyte was 1.0 M NaClO_4 in EC/PC (50/50 by volume) containing 5 wt% FEC. Different amounts of AAQ (0.04 – 0.12 wt%) were added to the liquid electrolyte. The electrolyte solution was prepared in a glove box filled with high-purity argon gas. The resulting liquid electrolyte was dried

* Corresponding author.

E-mail address: dongwonkim@hanyang.ac.kr (D.-W. Kim).

¹ M.-S. Park and J.-Y. Choi equally contributed to this work.

over molecular sieves to remove the residual water. The water content in the electrolyte was confirmed to be less than 25 ppm by Karl-Fischer titration.

2.2. Electrode preparation and cell assembly

NVPF was synthesized using a previously reported sol-gel method [11]. As depicted in Fig. S1, the X-ray diffraction pattern was well matched with a previously reported NVPF structure (JCPDS: 00-066-0321). The NVPF electrode was prepared by coating an N-methyl-2-pyrrolidone-based slurry containing 80 wt% NVPF, 10 wt% Ketjen black, and 10 wt% poly(vinylidene fluoride) binder on aluminum foil. The active mass loading in the electrode was approximately 5.0 mg cm^{-2} . A CR2032-type coin cell was assembled by sandwiching a glass fiber separator (ADVANTEC, GC-50) between sodium metal (Sigma-Aldrich) and the prepared NVPF electrode. A liquid electrolyte was then injected into the coin cell. All cells were assembled in a glove box filled with high-purity Ar gas.

2.3. Characterization and measurements.

Density functional theory (DFT) calculation was carried out with the Gaussian 16 to estimate the highest occupied molecular orbital (HOMO) and lowest unoccupied molecular orbital (LUMO) energy levels of AAQ, EC, PC and FEC [20,21]. All the calculations were performed with the hybrid functional B3LYP and the 6-311 + G(d,p) basis set. Cyclic voltammetry (CV) was conducted on a stainless-steel working electrode using a three-electrode system in the potential range of 2.0 to 4.3 V versus Na/Na^+ with a scan rate of 5.0 mV s^{-1} . Sodium foil and Pt wire were used as the reference and counter electrode, respectively. Before the cycle test of the Na/NVPF cell, the cell was subjected to three pre-conditioning cycles in the voltage range of 2.0 – 4.3 V at a constant current density of 10 mA g^{-1} using a battery cycler (WBCS 3000, Wonatech). The galvanostatic charge and discharge cycling test of the Na/NVPF cell was then performed in the same voltage range at 200 mA g^{-1} . AC impedance measurements of the cells were performed using a CH instrument (CHI 600D) over a frequency range of 5 mHz to 100 kHz with an amplitude of 5 mV. A galvanostatic intermittent titration technique (GITT) profile was obtained at a current density of 200 mA g^{-1} using the CHI 660D instrument. The chemical composition of thin layer formed on the NVPF electrode was investigated by XPS (VG Multilab ESCA system, 220i).

3. Results and discussion

Fig. S2 shows the HOMO and LUMO energy levels of AAQ, EC, PC and FEC. As can be seen in figure, AAQ has the highest HOMO energy level of -5.94 eV among solvents in the electrolyte solution, indicating its higher oxidation tendency prior to the oxidative decomposition of carbonate solvents (EC, PC and FEC) at the cathode during the charging processes. To confirm the electro-oxidative polymerization of AAQ in the liquid electrolyte, CV analysis was performed in the potential range of 2.0 – 4.3 V vs. Na/Na^+ . As shown in Fig. 1a, no significant oxidative current could be observed in the base electrolyte during anodic scan. Alternatively, the oxidative current started to increase near 4.0 V in the liquid electrolyte containing 0.06 wt% AAQ, as depicted in Fig. 1b. After repeating three cycles, a dark blue film was formed on the stainless-steel electrode in the AAQ-containing electrolyte, indicating that AAQ was electrochemically polymerized to form PAAQ on the working electrode. The oxidative current transforms AAQ into N^* radicals, which causes subsequent oxidation with AAQ molecules and chain propagation for polymerizing AAQ, as illustrated in Fig. 1c [19]. The electrochemical oxidation of AAQ results in the production of a conductive polymer film on the electrode because its polymerization product, PAAQ, is an electronically-conductive polymer in its oxidized state [22,23].

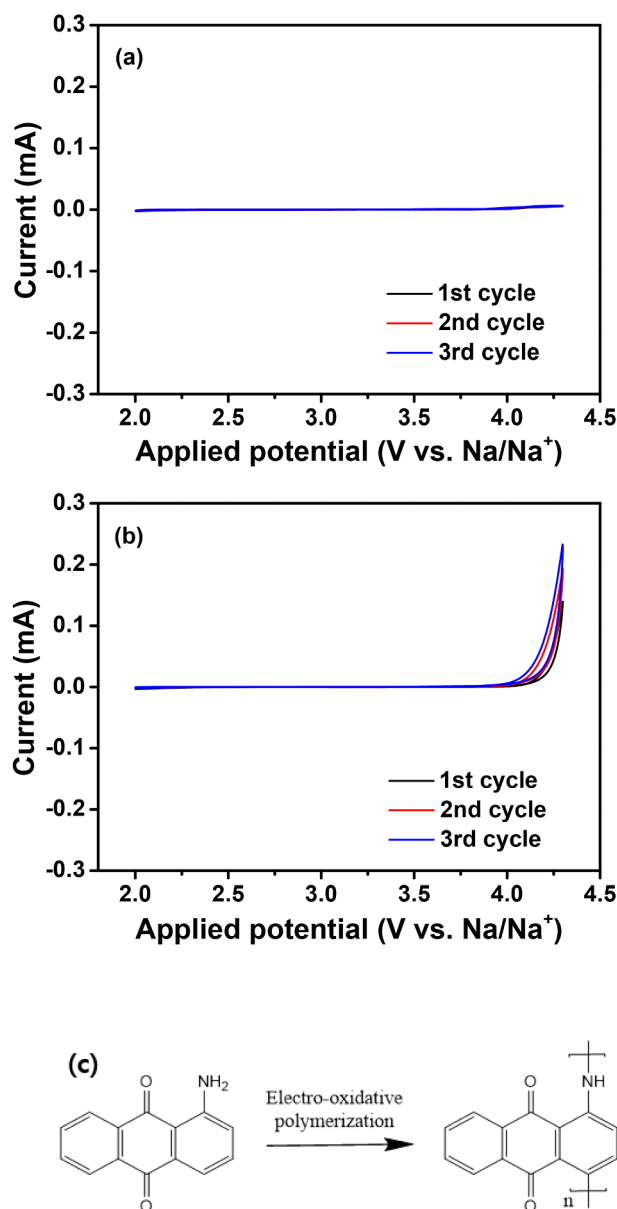


Fig. 1. Cyclic voltammograms of the three-electrode cells with different electrolytes at a scan rate of 5 mV s^{-1} : (a) liquid electrolyte without AAQ and (b) liquid electrolyte with 0.06 wt% AAQ. (c) Electro-oxidative polymerization of AAQ to PAAQ.

The morphology and chemical composition of the surface layer formed on NVPF were examined after pre-conditioning cycles of the Na/NVPF cell. Fig. 2a shows the charge-discharge curves of the Na/NVPF cells employing liquid electrolytes with and without AAQ during the first pre-conditioning cycle. The cells exhibited three well-defined plateaus with nearly the same discharge capacity of 119.2 mAh g^{-1} . Notably, the cell with 0.06 wt% AAQ showed lower Coulombic efficiency (81.0%) than the cell without AAQ (83.6%). The lower Coulombic efficiency in the cell with AAQ results from the irreversible oxidative polymerization of AAQ on the surface of NVPF during the charging process, because the oxidation of AAQ consumes a small amount of the capacity that corresponds to the irreversible capacity loss. Fig. 2b presents the TEM image of the NVPF particle obtained after the pre-conditioning cycles in the presence of 0.06 wt% AAQ, clearly indicating the NVPF particle was covered with a thin layer, and its thickness ranged from 16.7 to 35.8 nm. The chemical composition of the thin layer formed on NVPF was investigated by XPS analysis, as

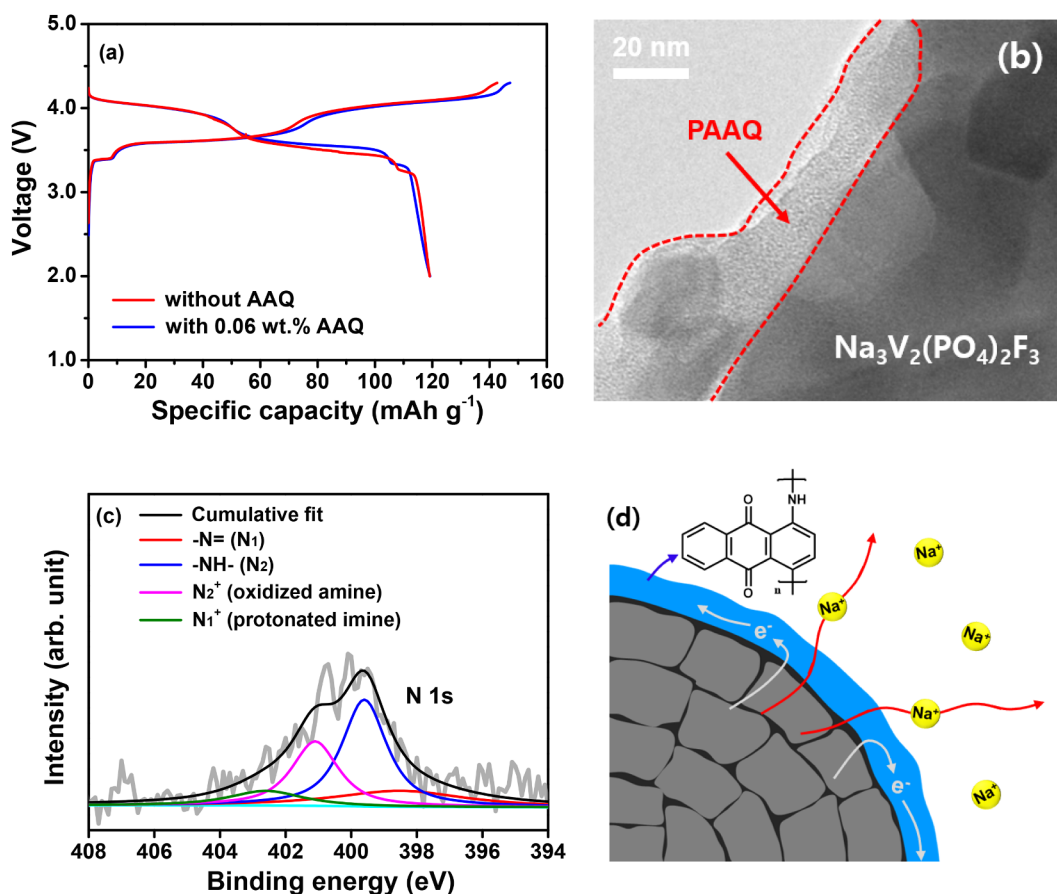


Fig. 2. (a) Charge and discharge profiles of the Na/NVPF cells employing liquid electrolytes without and with 0.06 wt% AAQ at the first pre-conditioning cycle. (b) TEM image of the NVPF particle after pre-conditioning cycles in the liquid electrolyte containing 0.06 wt% AAQ. (c) N 1s XPS spectrum of the NVPF electrode after pre-conditioning cycles. (d) Schematic presentation for enhancing the electrochemical performance of the NVPF cathode by formation of an electronically-conductive PAAQ layer.

shown in Fig. 2c. The N 1s spectrum shows four peaks, which correspond to quinoid imine (N₁, -N=, 398.5 eV), benzenoid amine (N₂, -NH-, 399.6 eV), protonated imine (N₁⁺, 402.6 eV), and oxidized amine (N₂⁺, 401.1 eV) [24–26]. The appearance of these chemical species verifies the formation of PAAQ via the electro-oxidative polymerization of AAQ on the NVPF cathode. Based on the XPS spectrum, the doping level (N⁺/N) in the PAAQ was calculated to be 37.3%, confirming that the obtained PAAQ had an electronically-conductive polymer structure. PAAQ had a higher doping level of 39.2% at fully charged state (Fig. S3), because the additional anion doping occurred during charging process [27]. These results indicate that PAAQ maintains its oxidized state and conductive nature during the whole charge/discharge processes. We also investigated the morphology and chemical composition of the NVPF without AAQ after pre-conditioning cycles. As shown in Fig. S4a, the TEM image of the NVPF cycled in the absence of AAQ exhibited a particle morphology without an additional surface layer. In the N 1s spectrum of the NVPF cathode without AAQ (Fig. S4b), no noticeable peaks could be observed, indicating that the electro-oxidative polymerization did not occur during cycling. The scheme in Fig. 2d illustrates the expected mechanism for enhancing the electrochemical performance of the NVPF cathode covered with the conductive PAAQ layer. The thin PAAQ layer provides the electron pathway during the charge and discharge cycles, which can facilitate the charge transfer reaction in the electrode.

The cycling performance of the Na/NVPF cell was evaluated at a

constant current density of 200 mA g⁻¹. Fig. 3a shows the charge and discharge curves of the cell assembled with liquid electrolyte containing 0.06 wt% AAQ. The cell with AAQ exhibited high and stable Coulombic efficiencies over 99.3% throughout cycling after initial cycles, which demonstrates good cycling stability of the cell with AAQ. When comparing the cycling performance of the cells with and without AAQ (Fig. 3b), the Na/NVPF cell with 0.06 wt% AAQ delivered a higher initial discharge capacity of 99.3 mAh g⁻¹ and a higher capacity retention of 85.6% after 100 cycles. On the other hand, the cell without AAQ exhibited an initial discharge capacity of 82.8 mAh g⁻¹ and a capacity retention of 81.6% at the 100th cycle. These results suggest that the thin conductive PAAQ layer formed on the NVPF cathode enhances the cycling performance in terms of discharge capacity and cycling stability. To understand the cycling behavior of the Na/NVPF cells, their AC impedance was measured after the pre-conditioning and 100 cycles, and the resulting AC impedance spectra are presented in Fig. 3c and d. In these spectra, the overlapped semicircle at high to medium frequency range was related to ion migration in the surface film (R_f) and charge transfer resistance (R_{ct}), and the sloping line in the low-frequency region is related to Na-ion diffusion in the electrode, as shown in the equivalent circuit (inset of Fig. 3d). The cell without AAQ showed a large increase in interfacial resistance (R_f + R_{ct}) from 134.3 to 172.4 Ω after cycling. The initial interfacial resistance of the cell with 0.06 wt% AAQ-containing electrolyte was much less (88.0 Ω) than the cell without AAQ, and the increase in the interfacial resistance after

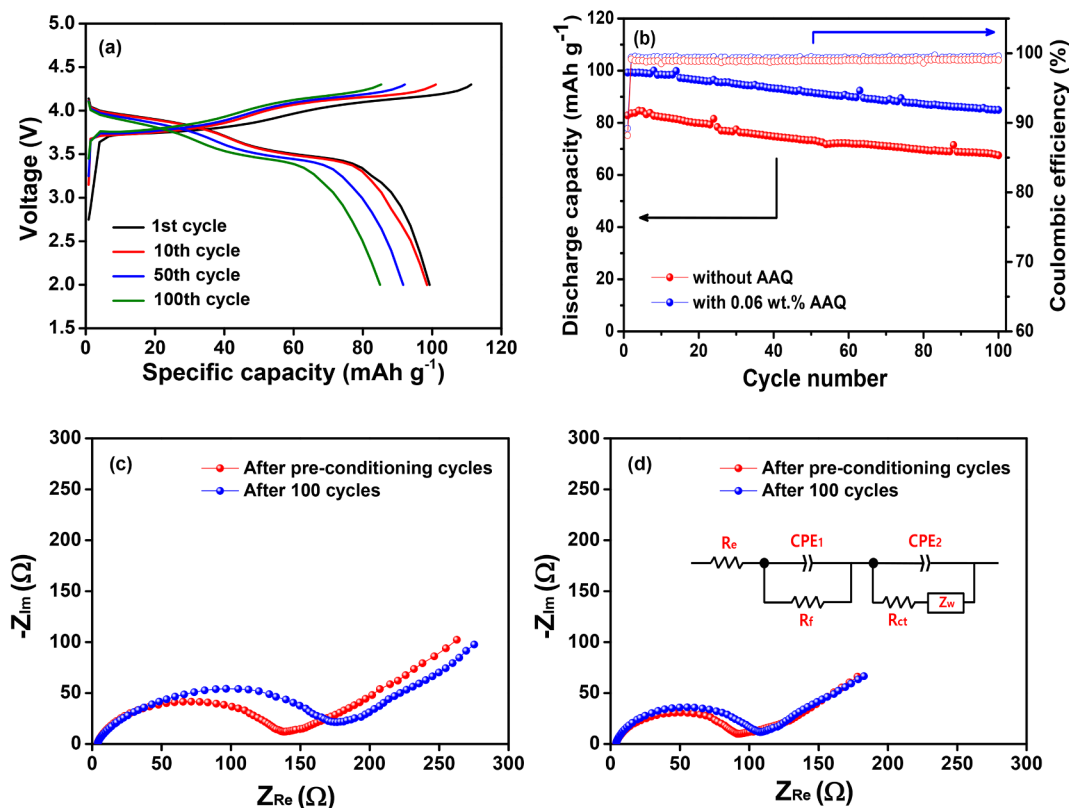


Fig. 3. (a) Charge and discharge curves of the Na/NVPF cell with liquid electrolyte containing 0.06 wt% AAQ and (b) cycling performance of the Na/NVPF cells employing liquid electrolyte without and with 0.06 wt% AAQ at 200 mA g^{-1} . AC impedance spectra of the Na/NVPF cells employing liquid electrolyte (c) without and (d) with 0.06 wt% AAQ.

cycling was relatively small. These results indicate that the thin PAAQ layer facilitates the charge transfer reaction of NVPF and thus decreases the interfacial resistance. Moreover, the conductive polymer film acts as a protective layer to reduce the oxidative decomposition of the electrolyte at high voltage, resulting in the stable interfacial resistances during cycling.

The rate capability of the Na/NVPF cells prepared with liquid electrolyte containing different amounts of AAQ was evaluated to investigate the influence of the PAAQ layer on the high rate performance of the NVPF cathode material. The cells were charged and discharged at various current densities from 50 to 2000 mA g^{-1} . Figs. 4a and S5a show the charge and discharge profiles of the Na/NVPF cells with and without AAQ (0.06 wt%) in the liquid electrolyte, respectively. The cell with 0.06 wt% AAQ exhibited higher discharge capacities than the cell employing base electrolyte at all the current densities. To compare the overpotential of the Na/NVPF cells with and without AAQ, the cell voltage was plotted as a function of the normalized capacity at 200 and 1000 mA g^{-1} in Fig. S5b and c, respectively. The overpotential of the cell with AAQ was lower than that of the cell with base electrolyte. When a conductive PAAQ layer formed on the surface of NVPF particles through the electrochemical polymerization of AAQ, it provides good electrical contact with the less conductive NVPF, which facilitates the electron transfer and decreases the overpotential of the electrode. The rate capability of the Na/NVPF cells with liquid electrolyte containing a different amount of AAQ was compared in Fig. 4b. The Na/NVPF cell with 0.06 wt% AAQ exhibited the highest discharge capacity at all of the current densities and delivered a discharge capacity of 61.1 mAh g^{-1} at a current density of 2000 mA g^{-1} . When the content of AAQ was greater than 0.06 wt%, a thick PAAQ layer (30.4 to

73.8 nm) was formed on the surface of the NVPF particle (Fig. S6), which restricts Na^+ transport from the electrolyte to the NVPF cathode and thus reduces the discharge capacity of the cell at high current densities. As a result, 0.06 wt% AAQ was an optimum content to achieve the best rate capability. The cycling performance of the Na/NVPF cell with 0.06 wt% AAQ was evaluated at higher current densities of 500 and 1000 mA g^{-1} . As shown in Fig. S7, the cell showed stable cycling behavior even at high current densities. We compared our results with those reported previously in Table S1. The NVPF cathode with 0.06 wt% AAQ exhibited good cycling stability and excellent rate capability as compared to those of the electrode materials previously reported. It demonstrates that the in-situ formation of a conductive PAAQ layer on the surface of the NVPF cathode with an addition of 0.06 wt% AAQ can be a promising approach for enhancing its electrochemical performance.

GITT analysis was performed to verify the beneficial effect of the conductive PAAQ layer on the electrochemical performance of the Na/NVPF cell. In GITT experiment, the pulse and relaxation time were 1 and 30 min, respectively (Fig. 5a). As shown in Fig. 5b, the cell with 0.06 wt% AAQ showed lower cell polarization and higher discharge capacity than the cell employing the base electrolyte. Considering the concentration polarization can be minimized with the GITT protocol, these results indicate that the formation of a thin conductive PAAQ layer on the NVPF facilitates the charge transfer reaction kinetics on the cathode material and thus enhances its electrochemical performance.

4. Conclusions

A small amount of AAQ was added to a liquid electrolyte as an

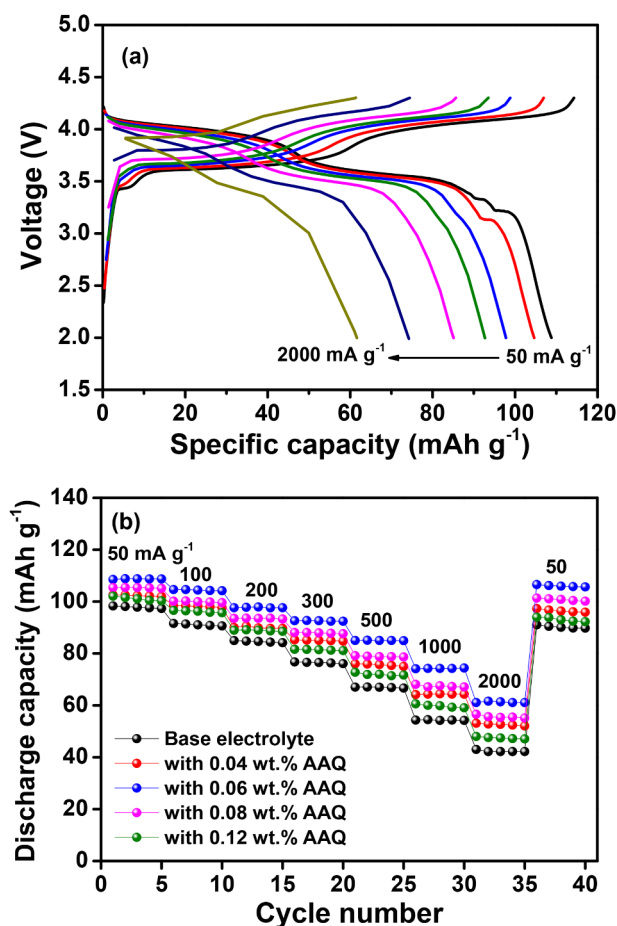


Fig. 4. (a) Charge and discharge curves of the Na/NVPF cell assembled with liquid electrolyte containing 0.06 wt% AAQ at different current densities. (b) Discharge capacities of the Na/NVPF cells assembled with liquid electrolytes containing different amounts of AAQ at various current densities.

electro-polymerizable additive. It was electrochemically oxidized to produce an electronically-conductive PAAQ on the surface of the NVPF cathode material. The formation of the conductive PAAQ layer reduced the interfacial resistance and suppressed the oxidative decomposition of the electrolyte during cycling. The concentration of 0.06 wt% AAQ was the most effective for improving the cycling performance of the Na/NVPF cell in terms of discharge capacity, cycling stability and rate capability. Our results demonstrate that the *in-situ* formation of a conductive PAAQ layer on the surface of the cathode material can be a simple and effective approach for enhancing its electrochemical performance.

CRediT authorship contribution statement

Myung-Soo Park: Conceptualization, Methodology, Writing - original draft. **Jin-Yi Choi:** Visualization, Investigation. **Ganesh Kumar Veerasubramani:** Formal analysis, Investigation. **Dong-Won Kim:** Supervision, Project administration, Funding acquisition.

Declaration of Competing Interest

The authors declare that they have no known competing financial interests or personal relationships that could have appeared to influence the work reported in this paper.

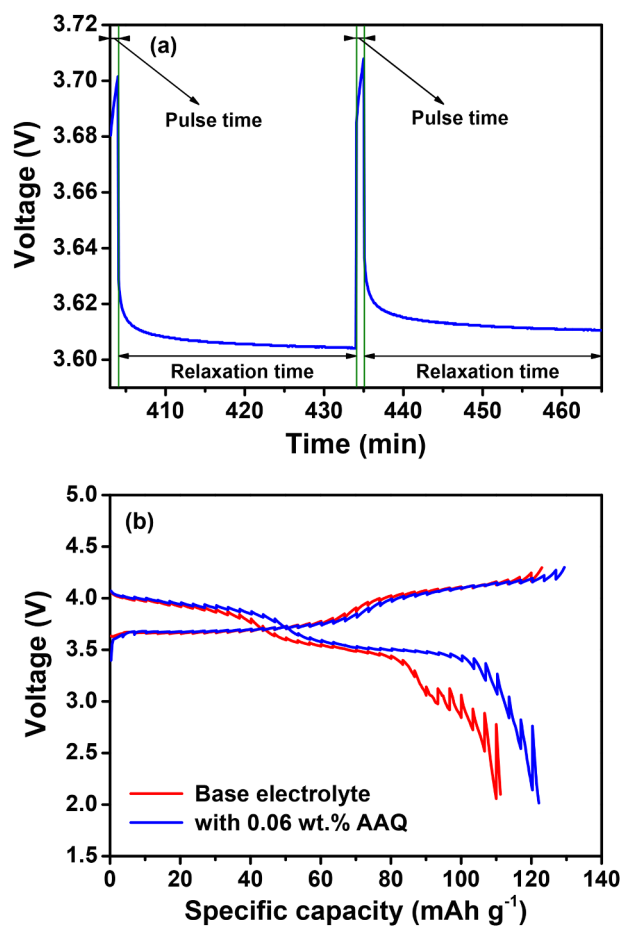


Fig. 5. (a) Cell voltage versus time for single GITT during the charging step and (b) GITT profiles of the Na/NVPF cells with different electrolytes.

Acknowledgements

This work was supported by the National Research Foundation of Korea (NRF) funded by the Korean Government (2019R1A4A2001527) and the Technology Innovation Program (20004958) funded by the Ministry of Trade, Industry and Energy (MOTIE).

Appendix A. Supplementary data

Supplementary data to this article can be found online at <https://doi.org/10.1016/j.elecom.2020.106829>.

References

- [1] M.D. Slater, D. Kim, E. Lee, C.S. Johnson, Sodium-ion batteries, *Adv. Funct. Mater.* 23 (2013) 947–958.
- [2] S.Y. Hong, Y. Kim, Y. Park, A. Choi, N.-S. Choi, K.T. Lee, Charge carriers in rechargeable batteries: Na ions vs. Li ions, *Energy Environ. Sci.* 6 (2013) 2067–2081.
- [3] N. Yabuuchi, K. Kubota, M. Dahbi, S. Komaba, Research development on sodium-ion batteries, *Chem. Rev.* 114 (2014) 11636–11682.
- [4] J.Y. Hwang, S.T. Myung, Y.K. Sun, Sodium-ion batteries: present and future, *Chem. Soc. Rev.* 46 (2017) 3529–3614.
- [5] R.A. Shakoor, D.-H. Seo, H. Kim, Y.-U. Park, J. Kim, S.-W. Kim, H. Gwon, S. Lee, K. Kang, A combined first principles and experimental study on Na₃V₂(PO₄)₂F₃ for rechargeable Na batteries, *J. Mater. Chem. A* 22 (2012) 20535–20541.
- [6] M. Nose, H. Nakayama, K. Nobuhara, H. Yamaguchi, S. Nakanishi, H. Iba, Na₄Co₃(PO₄)₂P₂O₇: a novel storage material for sodium-ion batteries, *J. Power Sources* 234 (2013) 175–179.
- [7] N. Yabuuchi, R. Hara, K. Kubota, J. Paulsen, S. Kumakura, S. Komaba, A new electrode material for rechargeable sodium batteries: P2-type Na_{2/3}[Mg_{0.28}Mn_{0.72}]

- O₂ with anomalously high reversible capacity, *J. Mater. Chem. A* 2 (2014) 16851–16855.
- [8] Y. Qi, L. Mu, J. Zhao, Y.-S. Hu, H. Liu, S. Dai, Superior Na-storage performance of low-temperature-synthesized Na₃(VO_{1-x}PO₄)₂F_{1+2x} nanoparticles for Na-ion batteries, *Angew. Chem., Int. Ed.* 54 (2015) 9911–9916.
- [9] Y. You, A. Manthiram, Progress in high-voltage cathode materials for rechargeable sodium-ion batteries, *Adv. Energy Mater.* 8 (2018) 1701785.
- [10] J.Y. Hwang, J. Kim, T.Y. Yu, Y.K. Sun, A new P2-type layered oxide cathode with extremely high energy density for sodium-ion batteries, *Adv. Energy Mater.* 9 (2019) 1803346.
- [11] Q. Liu, D. Wang, X. Yang, N. Chen, C. Wang, X. Bie, Y. Wei, G. Chen, F. Du, Carbon-coated Na₃V₂(PO₄)₂F₃ nanoparticles embedded in a mesoporous carbon matrix as a potential cathode material for sodium-ion batteries with superior rate capability and long-term cycle life, *J. Mater. Chem. A* 3 (2015) 21478–21485.
- [12] Q. Liu, X. Meng, Z. Wei, D. Wang, Y. Gao, Y. Wei, F. Du, G. Chen, Core/double-shell structured Na₃V₂(PO₄)₂F₃@C nanocomposite as the high power and long lifespan cathode for sodium-ion batteries, *ACS Appl. Mater. Interfaces* 8 (2016) 31709–31715.
- [13] L.-L. Zhang, D. Ma, T. Li, J. Liu, X.-K. Ding, Y.-H. Huang, X.-L. Yang, Polydopamine-derived nitrogen-doped carbon-covered Na₃V₂(PO₄)₂F₃ cathode material for high-performance Na-ion batteries, *ACS Appl. Mater. Interfaces* 10 (2018) 36851–36859.
- [14] Y. Cai, X. Cao, Z. Luo, G. Fang, F. Liu, J. Zhou, A. Pan, S. Liang, Caging Na₃V₂(PO₄)₂F₃ microcubes in cross-Linked graphene enabling ultrafast sodium storage and long-term cycling, *Adv. Sci.* 5 (2018) 1800680.
- [15] S. Liu, L. Wang, J. Liu, M. Zhou, Q. Nian, Y. Feng, Z. Tao, L. Shao, Na₃V₂(PO₄)₂F₃-SWCNT: a high voltage cathode for non-aqueous and aqueous sodium-ion batteries, *J. Mater. Chem. A* 7 (2019) 248–256.
- [16] X. Yang, X. Wang, W. Zhen, Reversible Na⁺-extraction/insertion in nitrogen-doped graphene-encapsulated Na₃V₂(PO₄)₂F₃@C electrode for advanced Na-ion battery, *Ceram. Int.* 46 (2020) 9170–9175.
- [17] Y. Li, X. Liang, G. Chen, W. Zhong, Q. Deng, F. Zheng, C. Yang, M. Liu, J. Hu, In-situ constructing Na₃V₂(PO₄)₂F₃/carbon nanocubes for fast ion diffusion with high-performance Na⁺-storage, *Chem. Eng. J.* 387 (2020) 123952.
- [18] A. Criado, P. Lavela, G. Ortiz, J.L. Tirado, C. Perez-Vicente, N. Bahrou, Z. Edfouf, Highly dispersed oleic-induced nanometric C@Na₃V₂(PO₄)₂F₃ composites for efficient Na-ion batteries, *Electrochim. Acta* 332 (2020) 135502.
- [19] W.A. Badawy, K.M. Ismail, S.S. Medany, Optimization of the electropolymerization of 1-amino-9,10-anthraquinone conducting films from aqueous media, *Electrochim. Acta* 51 (2006) 6353–6360.
- [20] Z.C. Zhang, L.B. Hu, H.M. Wu, W. Weng, M. Koh, P.C. Redfern, L.A. Curtiss, K. Amine, Fluorinated electrolytes for 5 V lithium-ion battery chemistry, *Energy Environ. Sci.* 6 (2013) 1806–1810.
- [21] J.-G. Han, E. Hwang, Y. Kim, S. Park, K. Kim, D.-H. Roh, M. Gu, S.-H. Lee, T.-H. Kwon, Y. Kim, N.-S. Choi, B.-S. Kim, Dual-functional electrolyte additives toward long-cycling lithium-ion batteries: ecofriendly designed carbonate derivatives, *ACS Appl. Mater. Interfaces* 12 (2020) 24479–24487.
- [22] X.-G. Li, H. Li, M.-R. Huang, M.G. Moloney, Synthesis and multifunctionality of self-stabilized poly(aminoanthraquinone) nanofibrils, *J. Phys. Chem. C* 115 (2011) 9486–9497.
- [23] K. Naoi, S. Suematsu, A. Manago, Electrochemistry of poly(1,5-diaminoanthraquinone) and its application in electrochemical capacitor materials, *J. Electrochem. Soc.* 147 (2000) 420–426.
- [24] Z. Tong, Y. Yang, J. Wang, J. Zhao, B.-L. Su, Y. Li, Layered polyaniline/graphene film from sandwich-structured polyaniline/graphene/polyaniline nanosheets for high-performance pseudosupercapacitors, *J. Mater. Chem. A* 2 (2014) 4642–4651.
- [25] S. Golczak, A. Kancierzewska, M. Fahlman, K. Langer, J.J. Langer, Comparative XPS surface study of polyaniline thin films, *Solid State Ionics* 179 (2008) 2234–2239.
- [26] R. Lin, S.K. Kaiser, R. Hauert, J. Perez-Ramirez, Descriptors for high-performance nitrogen-doped carbon catalysts in acetylene hydrochlorination, *ACS Catal.* 8 (2018) 1114–1121.
- [27] S. Lee, G. Kwon, K. Ku, K. Yoon, S.-K. Jung, H.-D. Lim, K. Kang, Recent progress in organic electrodes for Li and Na rechargeable batteries, *Adv. Mater.* 30 (2018) 1704682.